Supplementary material: Expanded Methods and Results

Accuracy of the volume pulsation quantification

In this Supplement, we further explain in detail how we studied the accuracy of the volume pulsation quantification analysis. The workflow is graphically supported by the flowchart in Supplementary figure 1.

1. The effect of contrast to noise ratio (CNR) and signal intensity fluctuations on the accuracy of the pulsation analysis, and the interaction with aneurysm size

In images with low CNR, the difference in intensity between the aneurysm and the background can be small. When using a signal intensity based segmentation method, the aneurysm volumes in these low CNR images could be overestimated. These artifactual volume changes resulting from signal fluctuations and low CNR, are due to a change in the detection of the border, and, thus depend on the size of the aneurysm or object.

Some systematic signal fluctuations over the heartbeat that are intrinsic to the acquisition method cannot be excluded, although these fluctuations were minimized by using cardiac gating in the TFE sequence, which means that the signal was maintained in steady state while waiting for the next electrocardiogram-R wave. Such signal fluctuations could be interpreted as a volume change by our segmentation method.

To study the effect of CNR and signal intensity fluctuations on the accuracy of the pulsation analysis, a spherical static digital phantom was simulated in Matlab R2013b (Mathworks, Natick, Massachusetts, USA). A graphical user interface was built to perform image analysis similar to the segmentation method used in the patient study (ANALYZE). The region of interest for segmentation of the phantom volume was standardized at twice the size of the phantom, and the signal intensity threshold for segmentation was chosen manually. To avoid the need for manual corrections of falsely included or excluded voxels after segmentation, a connected component analysis and a filling process were added to the image analysis. Using connected component analysis, the largest area of connected voxels in the image was preserved, while discarding all other single voxels. In the filling process, excluded pixels in the lumen of the phantom were automatically filled.

Contrast to noise ratio
To address the inaccuracy due to noise, images with decreasing contrast-to-noise ratio (CNR) were created. A static phantom with a diameter of 14 mm (volume of 1500 mm^3) was used, and noise was added by using the Rice distribution to simulate MRI-characteristic noise (1). Various amounts of noise were added to let the SNR of the phantom range in 15 steps between approx. 3 and 40.

Absolute (in mm^3) and relative volume pulsation were measured in the static phantoms in which CNR was varied, further referred to as the estimated inaccuracy of the volume pulsation analysis.

The results of this analysis showed that the effect of CNR on the estimated inaccuracy increases quickly below a CNR of approximately 6 (Supplementary figure 2).

The interaction of contrast to noise ratio (CNR) with aneurysm size (phantom volume) and its effect on the

accuracy of the pulsation analysis

The interaction of noise with the volume of the static phantom, was analyzed for three different CNRs: high (CNR≈12), medium (CNR≈4), and low (CNR≈2) CNR. Eleven static phantoms with increasing volumes (range 12-1500 mm^3) were used to study the interaction of CNR and aneurysm size (phantom volume). In these phantoms, the absolute (in mm^3) and relative volume pulsation was measured. The results of this analysis showed that in high CNR images, the image analysis performs flawlessly and independent of phantom size (Supplementary figure 3). In the phantoms with medium CNR, the estimated inaccuracy was small. The absolute estimated inaccuracy linearly increased with increasing phantom size (Supplementary figure 3, panel A). When analyzing the relative influence, a steep increase in estimated inaccuracy with decreasing phantom size was seen (Supplementary figure 3, panel B). Similar results were found in the phantom with low CNR, but with considerably larger absolute and relative inaccuracies (Supplementary figure 3).

Signal intensity fluctuations

To address the inaccuracy due to signal intensity fluctuations, we multiplied the static basic phantom intensity with a sine to create a sinusoidal intensity fluctuation throughout the fifteen time phases. The magnitude of the sine was varied between 0% and 10% of the phantom's mean intensity. In this analysis, the CNR level was kept high, with a mean CNR of 12. To simulate the MRI images and the inflow effect of blood realistically, a partial volume effect was introduced to the phantom images. First, a high-resolution phantom with 0.05 mm isotropic resolution (i.e. each voxel in the final phantom image contained 11 x 11 x 11 voxels in the high-resolution phantom) was rendered. Using Fast Fourier Transform, this high resolution phantom was converted from the spatial to the frequency domain (k-space). The k-space was cropped back to the original resolution. Subsequently, the cropped k-space was transformed back to the spatial domain using the inverse Fast Fourier Transform (Supplementary figure 4). Finally, noise was added to the image and image analysis was performed.

Absolute (in mm^3) and relative volume pulsation were measured in the static phantoms in which signal intensity was varied, further referred to as the estimated inaccuracy of the volume pulsation analysis. The results of this analysis showed that estimated inaccuracy increased with increasing intensity fluctuation (Supplementary figure 5).

The interaction of signal intensity fluctuations with aneurysm size (phantom volume) and its effect on the accuracy of the pulsation analysis

The interaction of phantom volume with the inaccuracy due to intensity fluctuations was also analyzed. This analysis was performed on the static phantom with three different sizes (large (volume of 1500 mm^3), medium (volume of 460 mm^3) and small (volume of 12 mm^3) size).
The results of the analysis of the interaction of size with intensity fluctuations are shown in Supplementary figure 5. The larger the phantom volume, the larger the absolute pulsation in the phantom (in mm^3, Supplementary figure 5, panel A). However, when looking at relative pulsation, small phantoms had a relatively larger inaccuracy than the larger phantoms (Supplementary figure 5, panel B).

2. Estimation of aneurysm-specific inaccuracy

As shown with the phantom measurements, both signal intensity fluctuations and CNR play a role in the inaccuracy of the measurement of actual aneurysm pulsation, and this inaccuracy depends on size of the phantom. To estimate the inaccuracy of each of the pulsation measurements in the patient study in stage I and stage II, an additional phantom experiment was performed.

Patient-specific pulsating phantoms were created, using an optimized version of the graphical user interface built to create static phantoms in Matlab (described above) The phantoms are spheres in a four dimensional space of 320x320x15x25 (respectively the x-coordinates, the y-coordinates, cardiac phases and slices). Volume pulsation was added to the phantoms with a linear increase and decrease of the volume with a maximum volume at the 8th cardiac phase. The amount of volume pulsation applied, was copied from the actual volume pulsation measured in each of the aneurysms with ANALYZE. For the aneurysms in stage II, we used the aneurysm volumes from the primary analysis in ANALYZE of the improved TFE sequence after contrast enhancement as input for the pulsating phantoms, because we assumed that the pulsation quantification on the images after contrast enhancement was the most accurate.
CNR of each of the aneurysms in our study was determined by using the equation shown above (Eq. S1) using a region of interest in the lumen of the aneurysm, and a region of interest in the background close to the aneurysm. The standard deviation of the noise was estimated as the standard deviation of the signal of the region of interest over the cardiac cycle. This will probably lead to slightly a higher noise level than actually present. Intensity fluctuations in the patient data was estimated at the edge of the aneurysms. First, a region of interest (red area in Supplementary figure 6) was encoded by eroding all slices in the 3D volume segmentations of the patient data (provided by ANALYZE) with a flat, disk-shaped structuring element with a radius of two voxels, resulting in an eroded region of interest. By subtracting the eroded region of interest from the segmentation, the edge of the aneurysm was determined (shown in green in Supplementary figure 6). The intensity fluctuation (ΔI) was calculated by:

$$\Delta I = \frac{[|I(t) - I_\mu|]_0^{t max}}{I_\mu} \qquad \text{[Eq. S2]}$$

where t represents the cardiac phases, $I(t)$ the mean pixel value in the edge of the region of interest for phase t and I_μ the mean pixel value over all the cardiac phases. The measured intensity fluctuations were applied to the phantoms in a sinusoidal shape where the measured fluctuation represents the amplitude of that sinus.

The volume pulsation of the pulsating phantom was determined with a signal intensity based threshold to automatically segment the phantom volume (comparable to the analysis in ANALYZE, but performed in Matlab, as described above). The difference between the volume pulsation input and the volume pulsation output of the phantoms was called the absolute observed artifactual pulsation. The magnitude of the absolute observed artifactual pulsation shows the inaccuracy of the pulsation analysis.

The results of the pulsating phantom analysis of the aneurysms in stage I of the study, show that in all but two aneurysms, the imaging analysis overestimated the volume pulsation (Supplementary table 1). In stage II, in all phantoms, the imaging analysis overestimated the volume pulsation (Supplementary table 2).

4. The effect of the flow displacement artifact on the accuracy of the pulsation analysis

The flow displacement artifact is another important determinant of the accuracy of the volume pulsation measurement in the patient data. This artifact is induced by flow in the phase encoding direction in between the time of phase encoding (directly after excitation) and frequency encoding (at t=TE), which causes misregistration. The effect of the flow displacement artifact on the volume pulsation quantification was estimated from the 3D phase contrast (PC)-MRI flow velocity data that was available for six of the ten aneurysms included in the current study (stage I). Briefly, the following scan parameters were used: field of view, 190 x 190 x 20 mm^3 (anterior to posterior x right to left x foot to head); acquired resolution, 0.5 x 0.5 x 0.5 mm^3; repetition time/ echo time, 8.5/7.1 milliseconds; and a flip angle of 20°. A velocity encoding of 150 cm/s in all directions was used. Six cardiac phases were obtained, retrospectively gated, using a peripheral pulse unit. The total scan duration was about 13 minutes, depending on the heart rate.

The magnitude of the PC-MRI data of a single heart phase was used as a mimic of the aneurysm as seen in the TFE sequence. Subsequently, the following formula was used to calculate the flow displacement artifact that would be present in the TFE sequence for each voxel of the aneurysm:

$$\Delta y_v = v_y(T_E - t_{pe})$$

where Δy_v represents the artefactual displacement in the phase encoding direction in a voxel, v_y is blood velocity in the phase direction, T_E is the echo time (4.4 ms for the TFE sequence), and t_{pe} the time of phase encoding (which was 1.6 ms for the TFE sequence, and obtained by inspecting the graphical sequence viewer supplied by the MRI vendor).

The calculated displacement artifact was applied to the magnitude of the PC-MRI data to simulate the flow displacement artifact of the TFE sequence. As the TFE sequence can be planned in any orientation with respect to the blood flow in the aneurysm, the phase encoding direction (in which the displacement artifact occurs) was simulated in three orthogonal directions, yielding three separate estimations of the potential flow displacement artifact. Before applying the displacement to the voxels of the PC-MRI magnitude image, this image was interpolated by a factor of 1000 in the simulated phase encoding direction to allow for sub-voxel shifts. Minimal aneurysm volume (V_{min}), maximum aneurysm volume (V_{max}) and the pulsation ($V_{pulsation}$) resulting from the flow displacement artifact was calculated for all available aneurysms and for the three different simulated orientations of the TFE sequence planning.

In five of the six aneurysms, the pulsation observed as a result of the flow displacement artifact was of the same magnitude or higher compared to the actual pulsation measured in the six available patient data sets, in at least one angulation (Supplementary table 3).

References
1. Henkelman RM. Measurement of signal intensities in the presence of noise in MR images. Med Phys 1985;12:232–233.

Supplementary table 1. The results of the volume pulsation quantification in pulsating phantoms. Phantom numbers correspond with the patients in Table 1 in the manuscript. The phantom input is the patient data obtained in Stage I of the study. CNR and intensity fluctuations were measured in the patient data and applied to the phantom. The phantom output is the result of the volume analysis of the pulsating phantom (mean of two times the analysis in Matlab).

Phantom	Phantom input					Phantom output			Absolute observed artifactual pulsation (mm^3)
	CNR	Intensity fluctuation (%)	Min volume (mm^3)	Max volume (mm^3)	Volume pulsation (mm^3)	Min volume (mm^3)	Max volume (mm^3)	Volume pulsation (mm^3)	
1	8	5.7	12	15	3	12.1	16.3	4.3	1.3
2	6	2.4	70	75	5	70.0	76.9	6.9	1.9
3	5	3.2	92	98	6	87.8	96.9	9.1	3.1
4	3	2.9	56	64	8	47.1	55.8	8.7	0.7
5	7	1.8	308	327	19	307.7	326.9	19.2	-0.2
6	6	2.1	292	303	11	292.4	302.3	9.9	1.1
7	3	6.7	285	298	13	276.6	295.0	18.4	5.4
8	1	2.7	276	298	22	276.1	297.7	21.6	-0.4
9	8	2.2	312	324	12	312.8	327.3	14.6	2.6
10	3	2.2	2078	2128	50	1987.8	2034.3	46.5	3.5

Supplementary table 2. Pulsation observed as result of the simulated flow displacement artifact (art) for three different orientations of the acquisition of the TFE sequence (phase encoding of the TFE sequence parallel to the x, y or z direction of the PC-MRI dataset, respectively). The actual pulsation as measured in the patient data (stage I) and the aneurysm size are shown at the bottom of the table.
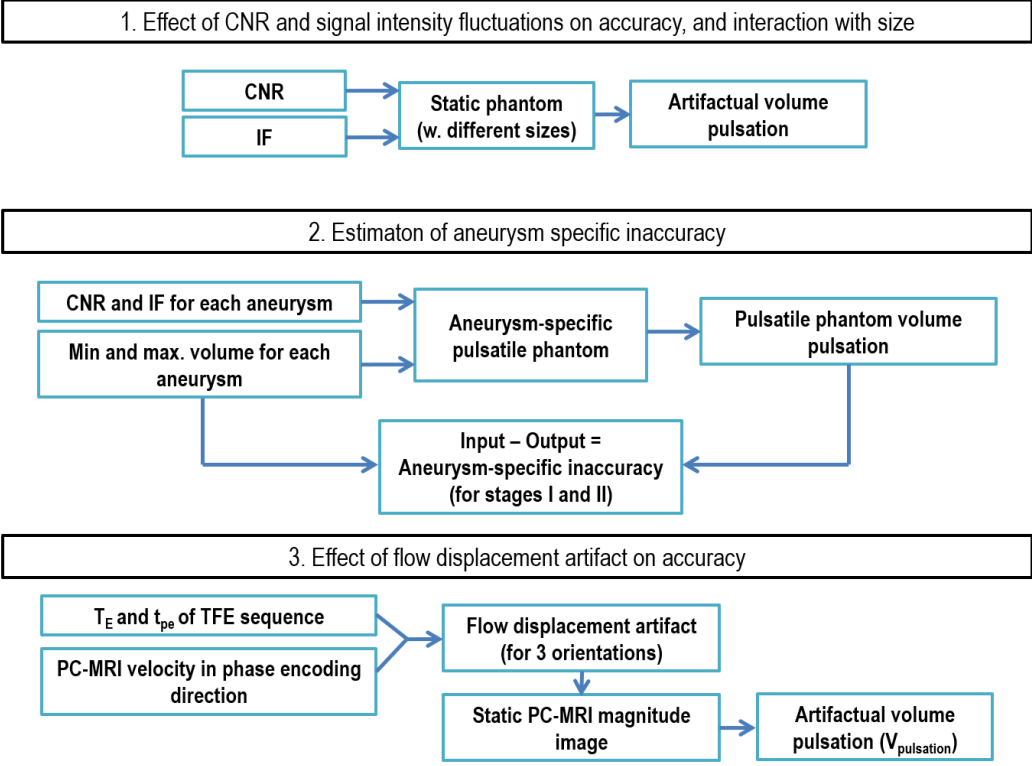
Orientation	Pulsation	Aneurysm 1	Aneurysm 2	Aneurysm 3	Aneurysm 4	Aneurysm 5	Aneurysm 6
[1,0,0]	V_{min} (art in mm^3)	141.4	212.6	174.4	506.0	731.2	596.5
	V_{max} (art in mm^3)	148.7	231.8	176.4	509.7	739.1	610.0
	$V_{pulsation}$ (art in mm^3)	7.3	19.2	1.9	3.7	7.9	13.5
[0,1,0]	V_{min} (art in mm^3)	133.9	183.0	179.6	508.6	729.4	591.9
	V_{max} (art in mm^3)	139.6	198.8	187.7	511.2	736.1	602.6
	$V_{pulsation}$ (art in mm^3)	5.7	15.8	8.1	2.7	6.8	10.7
[0,0,1]	V_{min} (art in mm^3)	138.1	182.4	179.6	495.1	720.7	588.7
	V_{max} (art in mm^3)	142.6	188.8	185.2	506.8	732.5	600.0
	$V_{pulsation}$ (art in mm^3)	4.5	6.4	5.6	11.7	11.7	11.2
	Aneurysm size (mm)	5.6	6.1	6.8	9.6	10.1	12.9
	V_{min} (in mm^3)	136.9	193.8	182.1	506.5	733.5	599.6
	$V_{pulsation}$ (in mm^3)	5	6	8	13	22	12

Supplementary table 3. The results of the volume pulsation quantification in pulsating phantoms of stage II.
Phantom numbers correspond with the patients in Table 2 in the manuscript. The phantom input is the patient data obtained in Stage II of the study. The aneurysm volumes from the primary analysis in ANALYZE of the improved TFE sequence after contrast enhancement were used as input for the pulsating phantoms, because we assumed that the pulsation quantification on the images after contrast enhancement was the most accurate. CNR and intensity fluctuations were measured in the patient data and applied to the phantom. The phantom output is the result of the volume analysis of the pulsating phantom (mean of two times the analysis in Matlab).
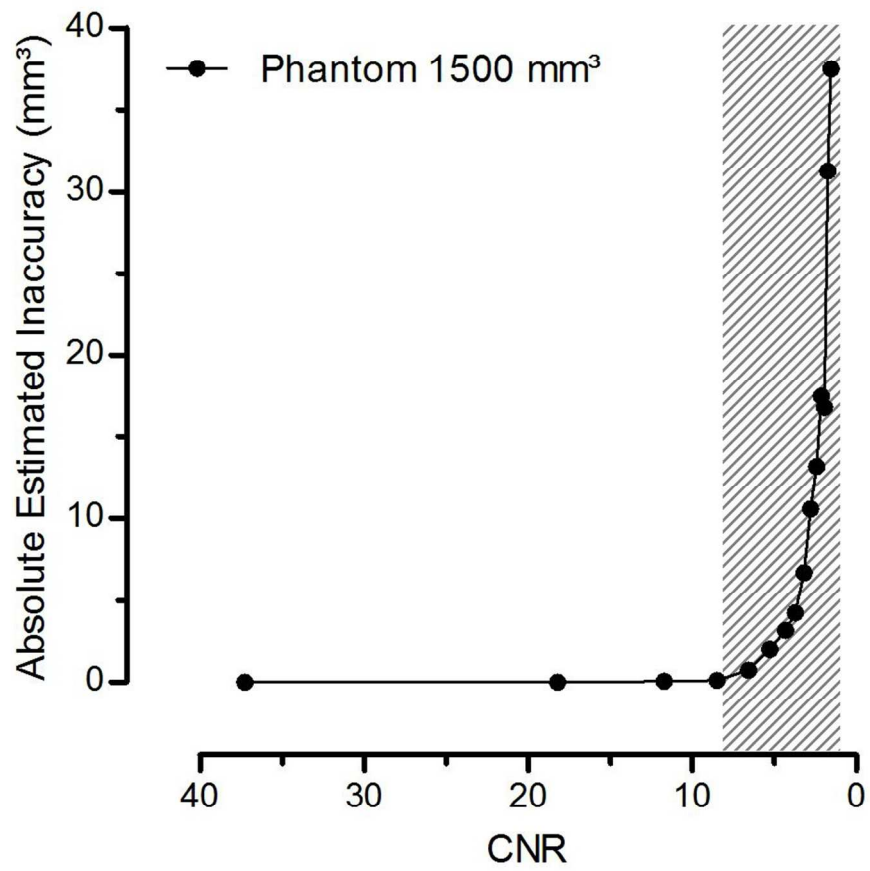A * indicates the phantom with the improved TFE sequence after contrast enhancement. In aneurysm 5, the image acquisition of the contrast enhanced improved TFE failed, and therefore, we were not able to perform a phantom analysis.

Phantom	Phantom input					Phantom output			Absolute observed artifactual pulsation (mm³)
	CNR	Intensity fluctuation (%)	Min volume (mm³)	Max volume (mm³)	Volume pulsation (mm³)	Min volume (mm³)	Max volume (mm³)	Volume pulsation (mm³)	
11	19	24	2	3	1	2	4	2	1
11*	44	22	2	3	1	1	4	3	2
12	29	20	96	104	8	93	102	9	1
12*	34	12	96	104	8	96	105	9	1
13	25	38	78	96	18	77	108	32	14
13*	19	24	78	96	18	73	104	31	13
14	18	22	70	78	8	68	84	16	9
14*	29	13	70	78	8	68	85	17	9
15	-	-	-	-	-	-	-	-	-
15*	-	-	-	-	-	-	-	-	-
16	39	30	114	138	25	113	164	50	26
16*	24	21	114	138	25	113	164	51	27
17	22	16	256	265	9	263	283	21	12
17*	23	10	256	265	9	263	282	19	10
18	19	18	166	191	25	156	203	47	22
18*	19	7.5	166	191	25	155	204	49	24
19	14	15	581	603	22	593	637	44	22
19*	28	8	581	603	22	553	600	47	25

1. Effect of CNR and signal intensity fluctuations on accuracy, and interaction with size

CNR

IF

Static phantom (w. different sizes)

Artifactual volume pulsation

2. Estimaton of aneurysm specific inaccuracy

CNR and IF for each aneurysm

Min and max. volume for each aneurysm

Aneurysm-specific pulsatile phantom

Pulsatile phantom volume pulsation

Input – Output = Aneurysm-specific inaccuracy (for stages I and II)

3. Effect of flow displacement artifact on accuracy

T_E and t_{pe} of TFE sequence

PC-MRI velocity in phase encoding direction

Flow displacement artifact (for 3 orientations)

Static PC-MRI magnitude image

Artifactual volume pulsation ($V_{pulsation}$)

Supplementary Figure 1

114x85mm (300 x 300 DPI)

Supplementary Figure 2
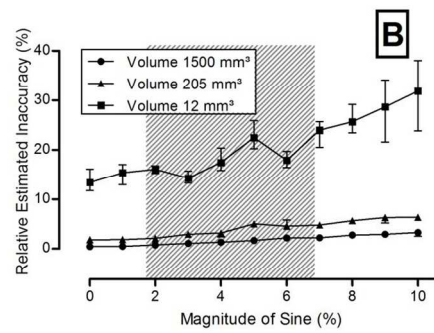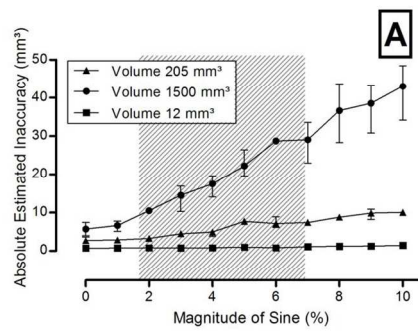
91x87mm (300 x 300 DPI)
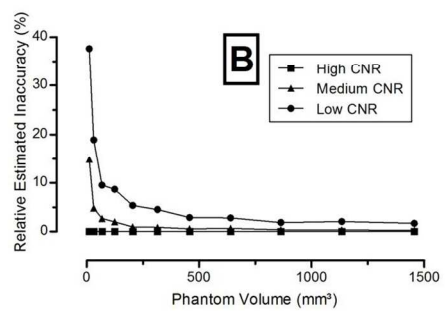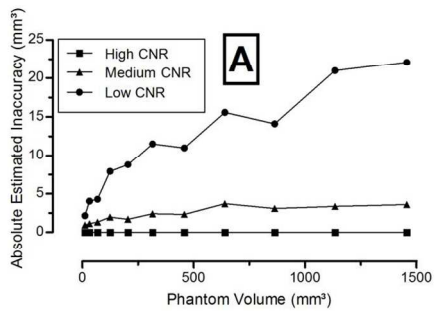
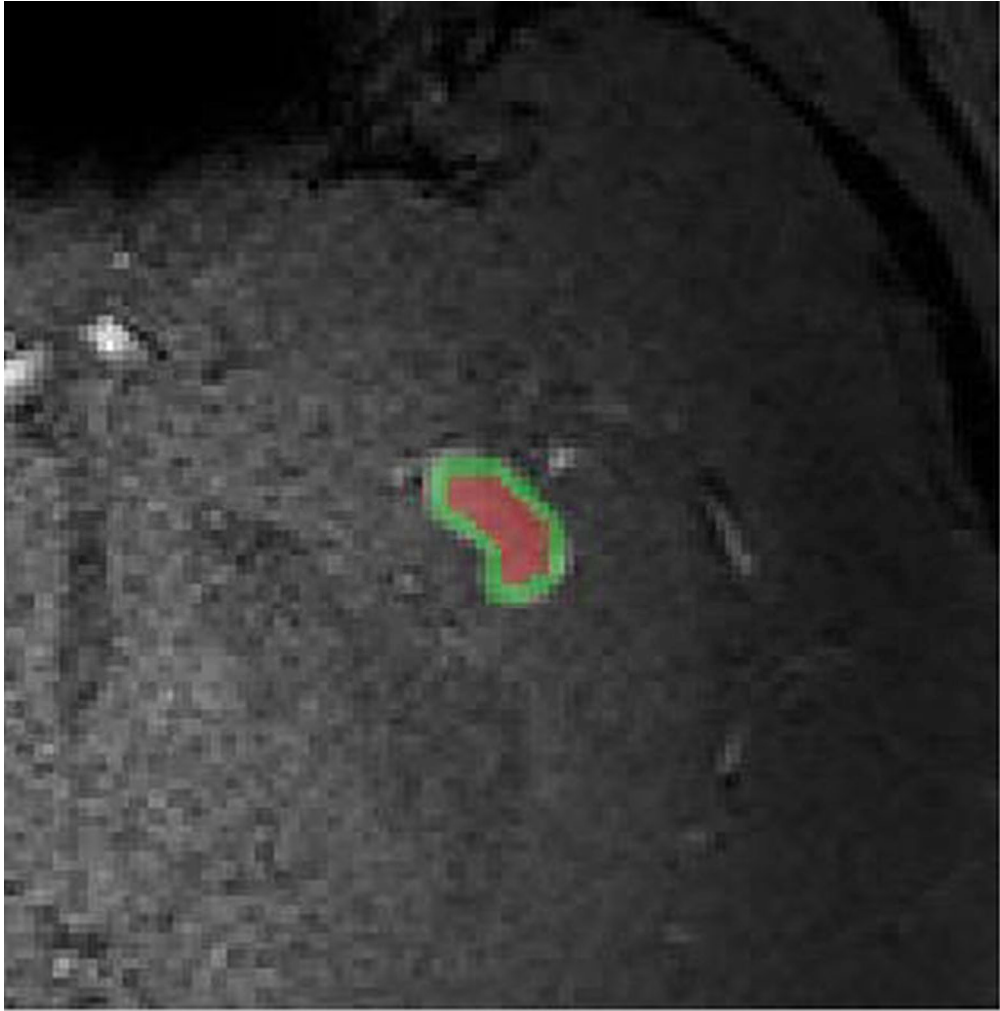Supplementary Figure 3

121x44mm (300 x 300 DPI)
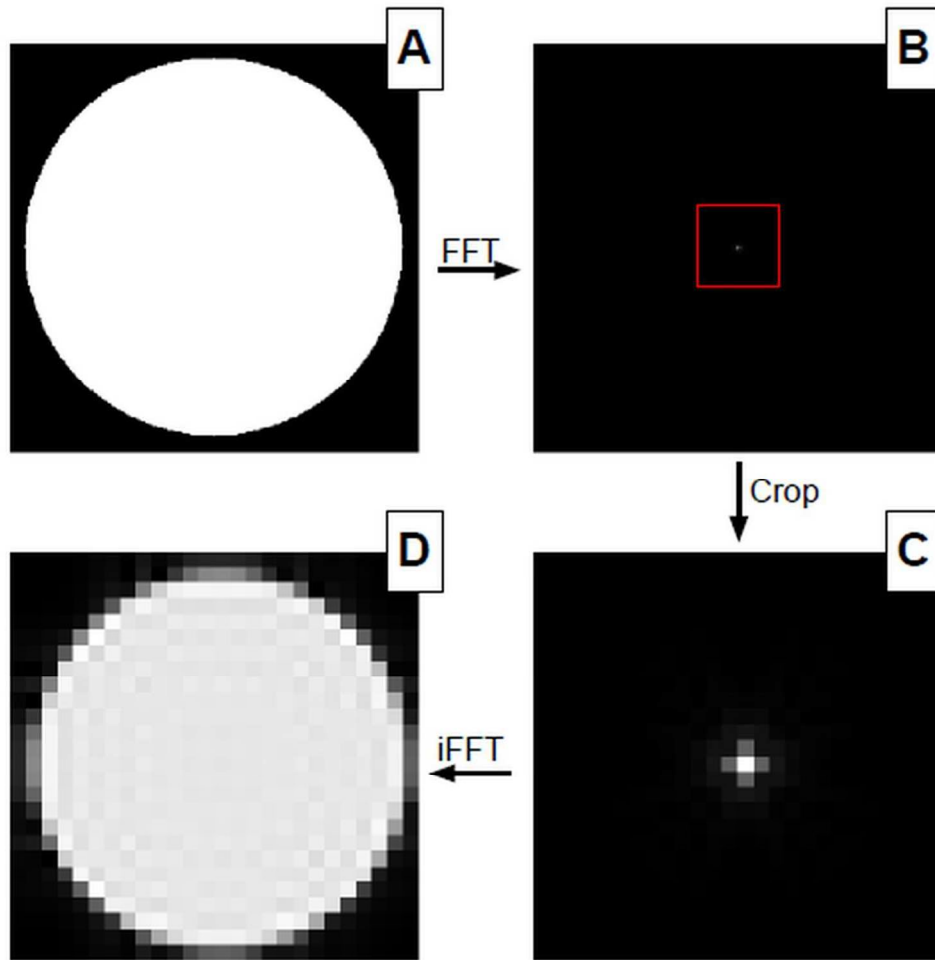
Supplementary Figure 4

101x100mm (300 x 300 DPI)

Supplementary Figure 5

121x44mm (300 x 300 DPI)

Supplementary Figure 6

76x76mm (300 x 300 DPI)

FIGURE LEGENDS

Supplementary material legend

Supplementary material: Expanded methods and results of the accuracy analysis of the measured volume pulsation studied by static digital phantom simulations.

Supplementary figure 1. Schematic overview of the accuracy analysis of the volume pulsation quantification.

Supplementary figure 2. Estimated inaccuracy of the volume pulsations analysis as function of the contrast-to-noise ratio (CNR). Measurement points indicate the decreasing CNR values as applied to the static phantom. The shaded area indicates the range of temporal CNRs measured in the patient scans of stage I, to indicate the for the patient study relevant range of CNRs.

Supplementary figure 3. The interaction of size of the phantom with CNR on the estimated inaccuracy of the volume pulsation measurement. The estimated inaccuracy is plotted against phantom volume in the static phantoms for three discrete CNRs, namely high CNR (CNR≈12), medium CNR (CNR≈4) and low CNR (CNR≈2). Graph A displays the influence of volume on the absolute estimated inaccuracy (mm^3), and graph B the influence of volume on the relative estimated inaccuracy (%).

Supplementary figure 4. Simulation of the partial volume effect in the phantom. A: a high resolution phantom; B: magnitude image of the frequency domain after applying the Fast Fourier Transform. The red square indicates the cropping area containing the low spatial frequencies; C: magnitude image of the frequency domain cropped back to the correct resolution; D: normal resolution phantom showing a clear partial volume effect, after applying the inverse Fast Fourier Transform.

Supplementary figure 5. Estimated inaccuracy of the volume pulsations analysis as function of the signal intensity fluctuations. The estimated inaccuracy of the analysis method was defined as the amount of observed pulsation in a static digital phantom.
(A) Absolute estimated inaccuracy versus the magnitude of sinusoidal brightness fluctuation in percentage of the mean signal and (B) relative estimated inaccuracy (relative is obtained by normalizing to mean volume) versus the sinusoidal brightness fluctuation in a simulated high-quality scan (CNR≈12) for three different phantom sizes. Shaded area indicates the range of brightness fluctuations measured in the patient scans in stage I of the patient study, to indicate the for the patient study relevant range of intensity fluctuations.

Supplementary figure 6. Intensity fluctuation measurement. A slice through a middle cerebral artery aneurysm with the eroded region of interest in red and the residual edge of the aneurysm in green.

Supplementary Video: Video showing volume pulsation of a middle cerebral artery aneurysm.

Coronal cross-section of a left middle cerebral artery aneurysm. Repetitive movie of the 15 phases of the cardiac cycle, showing volume pulsation of this aneurysm.